Time-dependent electric field fluctuations at the subphoton level

G. T. Foster,* W. P. Smith, J. E. Reiner, and L. A. Orozco
Department of Physics and Astronomy, State University of New York, Stony Brook, New York 11794-3800
(Received 27 May 2002; published 16 September 2002)

We report studies of a third-order correlation function that records the conditional time evolution of the field of a fraction of a photon. We present results in the strong-coupling regime of cavity QED, where the detection of a photon from the cavity prepares a state with a well-defined phase that evolves back to equilibrium via a damped vacuum Rabi oscillation. We perform a homodyne measurement conditioned on the photon detection to observe the regression of the field amplitude. The measured field-photon correlation is nonclassical and can be used to determine the spectrum of squeezing in an efficiency independent way.

DOI: 10.1103/PhysRevA.66.033807 PACS number(s): 42.50.Dv, 42.50.Ct, 32.80.−t

I. INTRODUCTION

Fluctuations of light have occupied quantum optics since its beginnings. The experimental studies have followed two broad lines: The first focuses on the intensity fluctuations and measures correlations between pairs of photon detections (particle aspect of light) [1–3], while the second kind studies squeezing that measures the fluctuation variance of the amplitude (wave aspect of light) [4–6].

Until recently these two classes of experiments remained separate, but now it is possible to combine them together in a modified approach that studies fluctuations of the electromagnetic field both theoretically [7] and experimentally [8]. This technique draws the particle and wave aspects together by correlating a photon detection with fluctuations of the electromagnetic wave amplitude, and introduces an additional third-order correlation function of the field. The relationship between quantum optical correlation functions and conditional measurements [3] underlies our approach which has been illuminated by quantum trajectory calculations [9]. Wiseman has shown the connection between the third-order correlation function and weak measurements in Ref. [10], while Denisov *et al.* [11] have explored the time symmetry properties of the correlation function that we study in this paper.

The light source we consider in this paper is a cavity quantum electrodynamic (QED) system. A single mode of the electromagnetic field interacts with a collection of N two-state atoms [12]. This source is known to emit nonclassical light; this has been demonstrated in both photon correlation [13–15] and squeezing measurements [16–18]. Other studies with intensity-field measurements have focused on the parametric down-conversion process, either as a generator of single-photon conditional states [19,20] or in an optical parametric oscillator [7,21].

The strong coupling of our cavity QED system allows us to observe the fluctuation in the wave amplitude of light [22,23]. By conditioning on a photon detection, we are able to observe the subsequent fluctuations as they occur. Because we use a normalized correlation function, the fluctuation is measured in its evolution over time in an efficiency-independent manner. Carmichael *et al.* [7] have shown that the full spectrum of squeezing can be obtained from this evolution. This is in contrast to the conventional way of measuring squeezing that suffers from detection efficiency loss.

The paper describes our experimental measurements, and we review the basic theoretical principles that underlie the experiments. The organization of the paper is as follows: Section II introduces the third-order correlation function and shows its application to the particular system of cavity QED. Section III describes the experimental apparatus and data taking procedures. Section IV presents the measurements, and Sec. V contains the conclusions.

II. THEORY

Figure 1 shows the general schematic of the field-intensity correlator. It is based on the implementations of the Hanbury-Brown and Twiss intensity correlator with the ''start''/''stop'' scheme [15]. The main difference is the balanced homodyne detector that replaces the photon detector (photomultiplier tube, or avalanche photodiode), in the ''stop'' channel. Within a few correlation times before and after each ''start,'' the homodyne current $I(t)$ is digitized, recorded, and used to update a cumulative average. Averaging N_s such samples reduce the shot noise; the surviving signal is a conditional average of the quadrature amplitude fluctuations.

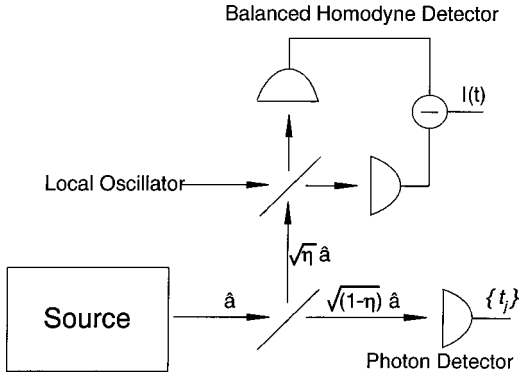

FIG. 1. Schematic of field-intensity correlator.

*Present address: Department of Physics, Yale University, New Haven, CT 06520-8120.

A. The third order correlation function

Consider a general optical source with a power bandwidth of 2κ and nonzero steady-state average field. We send a fraction η to a homodyne detector and the remaining $1-\eta$ to a photon detector (see Fig. 1). The photon flux operator at the photon detector is given by the number operator on the source field [7],

$$\hat{S}=(1-\eta)2\kappa\hat{a}^{\dagger}\hat{a}. \tag{1}$$

This gives the starts for a homodyne detector. The homodyne detector samples the quadrature phase amplitude that is in phase with a local oscillator (LO) field,

$$\hat{D}=\sqrt{\eta}\sqrt{2\kappa}[\hat{a}e^{-i\theta}+\hat{a}^{\dagger}e^{i\theta}]. \tag{2}$$

The conditional homodyne photocurrent ensemble averaged over many starts is given by

$$H_{\theta}(\tau)=\frac{\langle:\hat{S}(t)\hat{D}(t+\tau):\rangle}{\langle\hat{S}\rangle}+\xi(t), \tag{3}$$

with $\langle::\rangle$ denoting time and normal ordering. $\xi(t)$ is residual local oscillator shot noise since we only average over a finite number of samples.

When the electromagnetic field of interest is small and nonclassical, its fluctuations, a manifestation of the uncertainty principle, dominate over the steady-state amplitude [24]. The field operator $\hat{a}$ is better described by $\hat{a}=\alpha+\Delta\hat{a}$, with $\alpha=\langle\hat{a}\rangle=|\alpha|e^{i\phi}$ and $\Delta\hat{a}$ a fluctuation. In this way, we can follow the influence of the fluctuations in the quantities we compute or measure. We can evaluate Eq. (3) by substituting Eqs. (1) and (2) and separating the field into its mean and fluctuations. We make one further assumption that is clearly valid for the case of Gaussian fluctuations, that third-order moments are zero, but as Denisov *et al.* have shown [11], this is not a necessary requirement and it is directly related to the assumptions of detailed balance. The resulting correlation function is

$$H_{\phi\theta}(\tau)=\sqrt{2\kappa\eta}|\alpha|\left(2\cos(\phi-\theta)+\frac{2\langle:\Delta\hat{a}_{\phi}\Delta\hat{a}_{\theta}(\tau):\rangle}{|\alpha|^2+\langle\Delta\hat{a}^{\dagger}\Delta\hat{a}\rangle}\right)+\xi(t). \tag{4}$$

With the mean field in phase with the local oscillator ($\phi=\theta$), we obtain a normalized correlation function by dividing Eq. (4) by the mean field $\sqrt{2\kappa\eta}|\alpha|$ [7],

$$h_{\theta}(\tau)=1+\frac{2\langle:\Delta\hat{a}_{\theta}\Delta\hat{a}_{\theta}(\tau):\rangle}{|\alpha|^2+\langle\Delta\hat{a}^{\dagger}\Delta\hat{a}\rangle}+\frac{\xi(t)}{\sqrt{2\kappa\eta}|\alpha|}. \tag{5}$$

$h_{\theta}(\tau)$ can be factorized with the help of the quantum regression theorem [23] into $h_{\theta}(\tau)=\langle\hat{E}(\tau,\theta)\rangle_c/\langle\hat{E}(t)\rangle$, the normalized field amplitude conditioned upon the detection of a photon.

The spectrum of squeezing for the field quadrature in phase with the mean field is

$$S(\Omega,0^{\circ})=4F\int_0^{\infty}d\tau\cos(2\pi\Omega\tau)[\overline{h}_{0^{\circ}}(\tau)-1], \tag{6}$$

where $F=2\kappa\langle\hat{a}^{\dagger}\hat{a}\rangle$ is the source photon flux and $\overline{h}_{0^{\circ}}(\tau)$ is the measured $h_{0^{\circ}}(\tau)$ in the limit of vanishing shot noise. This allows the time-resolved measurement of the amplitude fluctuations of the squeezed electromagnetic field. Notice that the normalized correlation h_{θ} is independent of the detection and coupling efficiency. The squeezing spectrum does depend on the quantum efficiency of the photon detector used to measure the source flux. This technique is less sensitive to efficiencies than traditional squeezing measurements [26] since the propagation losses are taken into account by the normalization of $h_{\theta}(\tau)$.

Squeezing measurements are directly related to a reduction in the variance of one of the field quadratures. This can manifest itself through violations of the classical bounds set on the correlation function h_{θ}. We present the derivation of two such classical bounds here following the work of Carmichael *et al.* in Ref. [7].

We begin by rewriting the fluctuations of the two-field quadratures as follows:

$$\langle\Delta\hat{a}^{\dagger}\Delta a\rangle=\langle:\Delta\hat{a}_{\theta}^2:\rangle+\langle:\Delta\hat{a}_{\theta+\pi/2}^2:\rangle. \tag{7}$$

Combining Eq. (5) with Eq. (7) leads to an expression for h_{θ} at $\tau=0$,

$$h_{\theta}(0)-1=\frac{2\langle:\Delta\hat{a}_{\theta}^2:\rangle}{(\langle:\Delta\hat{a}_{\theta}^2:\rangle+\langle:\Delta\hat{a}_{\theta+\pi/2}^2:\rangle)\left(1+\dfrac{\alpha^2}{\langle\Delta\hat{a}^{\dagger}\Delta\hat{a}\rangle}\right)}. \tag{8}$$

In the classical case, both quadrature variances are greater than zero, so from Eq. (8) we get the following upper and lower bounds for $h_{\theta}(0)$:

$$0\leq h_{\theta}(0)-1\leq\frac{2}{\left(1+\dfrac{\alpha^2}{\langle\Delta\hat{a}^{\dagger}\Delta\hat{a}\rangle}\right)}. \tag{9}$$

This may be generalized for nonzero values of time. We begin by stating the Schwarz inequality

$$|\langle:\Delta\hat{a}_{\theta}\Delta\hat{a}_{\theta}(\tau):\rangle|^2\leq\langle:\Delta\hat{a}_{\theta}^2:\rangle\langle:\Delta\hat{a}_{\theta}^2(\tau):\rangle. \tag{10}$$

This implies the following inequality:

$$|h_{\theta}(\tau)-1|^2\leq\frac{\langle:\Delta\hat{a}_{\theta}^2:\rangle\langle:\Delta\hat{a}_{\theta}^2(\tau):\rangle}{|\alpha^2+\langle\Delta\hat{a}^{\dagger}\Delta\hat{a}\rangle|^2}, \tag{11}$$

which is equivalent to

$$|h_\theta(\tau)-1| \leqslant |h_\theta(0)-1|. \tag{12}$$

This second Schwarz condition is similar to that associated with photon antibunching [2].

B. Cavity QED system

The cavity QED system consists of a single mode of the electromagnetic field interacting with a collection of two-level atoms. The atom-cavity coupling rate is given by

$$g_0 = \left(\frac{\mu^2 \omega}{2\hbar \epsilon_0 V} \right)^{1/2} \tag{13}$$

for cavity mode volume V and atomic transition frequency ω and dipole moment μ. Dissipation plays an important role as both the atoms and the field couple to reservoirs. An atom can spontaneously emit light into modes other than the preferred cavity mode, and light inside the cavity can escape through the mirrors. Dissipation occurs through the decay of energy from the cavity at rate κ and the decay of the atomic inversion $\gamma_\parallel = 1/\tau$ (τ is the radiative lifetime of the atomic transition) and polarization $\gamma_\perp$. For purely radiative decay, $\gamma_\parallel = 2\gamma_\perp$. We drive the system with a field injected through one of the mirrors and detect the light that escapes from the cavity mode through the output mirror.

Work on optical bistability (OB) [25] produced a large amount of experimental and theoretical literature on the transmission properties of an optical cavity filled with two-level atoms. Two dimensionless numbers from the OB literature are useful for characterizing cavity QED systems: the saturation photon number n_0 and the single-atom cooperativity C_1. Defined as $n_0 = 2\gamma_\perp \gamma_\parallel / 3g_0^2$ and $C_1 = g_0^2/2\kappa\gamma_\perp$, they scale the influence of a photon and the influence of an atom in the system. The strong-coupling regime of cavity QED $n_0 < 1$ and $C_1 > 1$ implies very large effects from the presence of a single photon and of a single atom in the system.

The equilibrium state of the atom-cavity system is significantly altered by the escape of a photon. The dynamics consists of a collapse of the system state $|\psi\rangle$ followed by a damped Rabi oscillation back to equilibrium. We are interested in the reduction of the equilibrium state of the cavity QED system after detecting a photon emitted from the cavity mode (see Fig. 1). Defining $\hat{A}_\theta \equiv [\hat{a}\exp(-i\theta) + \hat{a}^\dagger \exp(i\theta)]/2$, where $\hat{a}$ is the annihilation operator for the cavity field and θ is the homodyne detector phase, we consider the quadrature amplitude, $\hat{A}_{0^\circ}$, in phase with the steady state of the field $\lambda \equiv \langle a \rangle$. We limit our discussion to the case where the cavity and laser are resonant with the atomic transition. For weak excitation, and assuming fixed atomic positions the equilibrium state to second order in λ is the pure state [22,23]

$$|\psi_{SS}\rangle = [|0\rangle + \lambda|1\rangle + (\lambda^2/\sqrt{2})\chi\beta|2\rangle + \cdots]|G\rangle + [\rho|0\rangle + \lambda\rho\beta|1\rangle + \cdots]|E\rangle + \cdots, \tag{14}$$

where $|G\rangle$ is the N-atom ground state and $|E\rangle$ is the symmetrized state for one atom in the excited state with all others in the ground state. We assume that all the N atoms are coupled to the cavity mode with the same strength, g_0, with χ, β, and ρ derived from the master equation in the steady state [22],

$$\chi = 1 - 2C_1' \;;\; \beta = \frac{1+2C}{1+2C-2C_1'} \;;\; \rho = -\frac{\sqrt{N} g_0 \lambda}{\gamma_\perp}, \tag{15}$$

where

$$C \equiv NC_1, \quad C_1' \equiv \frac{C_1}{(1+\gamma_\perp/\kappa)}. \tag{16}$$

After detecting the escaping photon, the conditional state is initially the reduced state $\hat{a}|\psi\rangle/\lambda$, which then relaxes back to equilibrium. The reduction and regression is traced by [22,23]

$$|\psi\rangle \rightarrow \{|0\rangle + \lambda[1 + \mathcal{A}F(\tau)]|1\rangle + \cdots\}|G\rangle + \cdots, \tag{17}$$

where

$$\mathcal{A} = -\frac{4C_1'C}{1+2C-2C_1'}, \tag{18}$$

$$\mathcal{F}(\tau) = \exp\left(\frac{-(\kappa+\gamma_\perp)\tau}{2} \right) \left(\cos\Omega_0\tau + \frac{\kappa+\gamma_\perp}{2\Omega_0} \sin\Omega_0\tau \right), \tag{19}$$

$$\Omega_0 = \sqrt{g_0^2 N - \frac{1}{4}(\kappa-\gamma_\perp)^2}. \tag{20}$$

From Eqs. (14) and (17) we see that after a photodetection, the quadrature amplitude expectation makes the transient excursion $\langle \hat{A}_{0^\circ}(\tau) \rangle \rightarrow \lambda[1 + \mathcal{A}F(\tau)]$ away from its equilibrium value $\langle \hat{A}_{0^\circ} \rangle = \lambda$.

In the weak-field limit, which assumes up to two excitations in the steady state of the system, the conditional field measurement is

$$h_\theta(\tau) = [1 + \mathcal{A}F(\tau)]\cos\theta. \tag{21}$$

The correlation function measures the coefficient of the single-photon state in Eq. (17); it is usually a very small number and it is appropriate to talk of a field fluctuation at the subphoton level. $\mathcal{A}$ is the relative change of the field inside the cavity caused by the escape of a photon [9,22]: The limit of large N gives $\mathcal{A} \approx -2C_1/(1+\gamma_\perp/\kappa)$, showing the importance of the single-atom cooperativity as the parameter that establishes the nonclassicality of the field. The sign of $\mathcal{A}$ tells us that the cavity field goes negative causing a possible reduction. The jump occurs because the polariza-

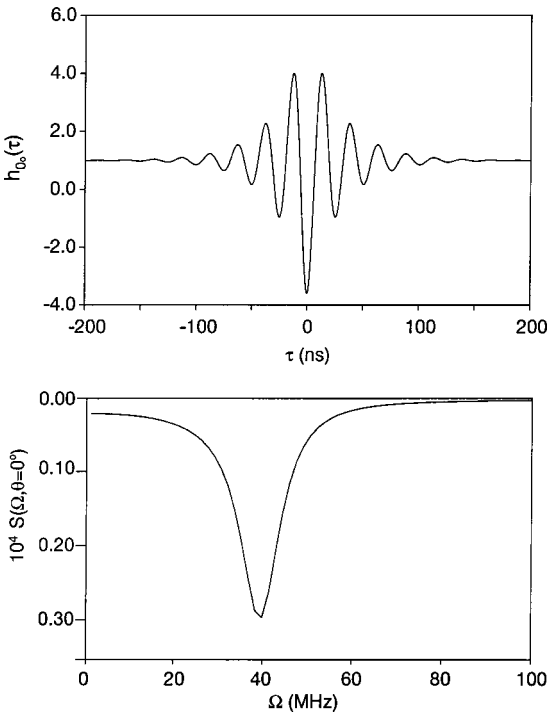

FIG. 2. Top: $h_{0^\circ}(\tau)$ calculation for 11 atoms maximally coupled. Bottom: Normalized spectrum of squeezing. $(g_0,\kappa,\gamma_\perp)/2\pi=(12,8,3)$ MHz.

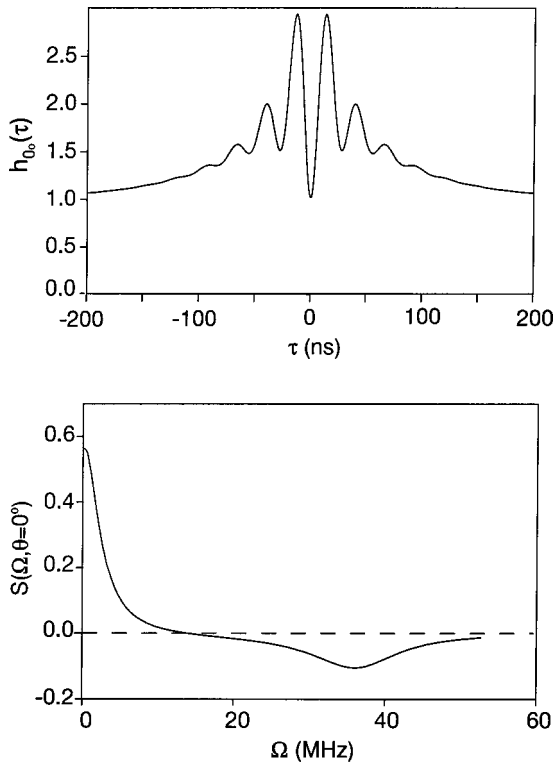

FIG. 3. Top: $h_{0^\circ}(\tau)$ for $N=2$ atoms beyond the low-intensity regime. Bottom: squeezing spectrum from the correlation function above.

tion of the medium increases when a photon leaves the cavity. The collective cavity enhancement of the dipole decay rate is reduced by the ratio $(N-1)/N$ and this increases the polarization amplitude (which is inversely proportional to the damping rate).

We are not sensitive to in-quadrature fluctuations because on resonance, as established in OB, the mean field is zero at $\theta=90°$. A mean field of zero does not permit normalization of the correlation function as we do in Eq. (5). A possible way to get to the other quadrature component of the fluctuations is by adding a coherent offset to the signal before sending it to the start detector and homodyne detector to provide a mean field to allow triggers at that phase [7]. Another way would be to operate with the system off-resonance to ensure that there is a steady-state field in the other quadrature.

C. Predictions and refinements of the model

The analytical expressions for the behavior of the system are based on assumptions that all atoms are at rest, maximally coupled to the cavity field mode, and under weak excitation. Our experimental implementation involves an atomic beam that places an ensemble of moving atoms at random positions in the cavity mode. Our experiment also may not operate in the regime of weak excitation. We would hope that the analytic expressions still provide a qualitative prediction of what we would expect. To completely model the effects of our experimental regime, a full atomic beam quantum Monte Carlo simulation would be required. We can gain significant insight with somewhat less involved numerical studies that refine the model by taking into account an increased driving field intensity, the spatial distribution of the atoms inside the cavity mode, and the transit time of the atoms across the cavity mode. We now show how each of these refinements, considered individually, lead to the modification of the maximally coupled, weak-field results of the preceding section.

1. Low intensity

We begin by plotting the conditioned field evolution in the low-intensity regime, $n/n_0 \ll 1$, where Eq. (21) applies. The top of Fig. 2 shows the calculation of $h_{0^\circ}(\tau)$ for 11 atoms maximally coupled to a cavity in a system with $(g_0,\kappa,\gamma_\perp)/2\pi=(12,8,3)$ MHz. The parameters are similar to those of our experiments. The correlation function violates the two Schwarz inequalities of Eqs. (9) and (12). The bottom of Fig. 2 shows the corresponding Fourier transform of the correlation. Squeezing, a nonclassical effect, appears at a frequency close to the coupling constant $(g_0\sqrt{N})$ with a width of the average of the decay processes $[(\kappa+\gamma_\perp)/2]$.

2. Higher intensity

Figure 3 shows the result for two atoms maximally coupled to the cavity mode with a drive that corresponds to a steady-state intracavity intensity of $n/n_0=18$, far from the low-intensity limit. We carry out numerical calculations with a larger basis that takes into account more excitations [9,30]. The coupling constant g_0 produces a similar vacuum Rabi oscillation Ω_0 as that of Fig. 2. The background that is visible around $\tau=0$ comes from the spontaneously emitted pho-

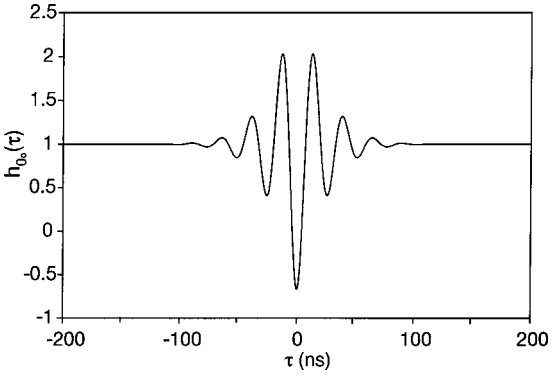

FIG. 4. Averaged $h_{0\circ}(\tau)$ with $N=190$ fixed atoms in the mode volume coupled according to the distribution from Eq. (22).

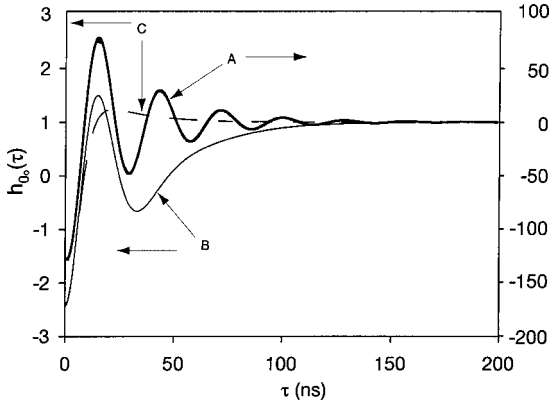

FIG. 5. $h_{0\circ}(\tau)$ calculation for one atom coupled to a 35 μm waist cavity, with three different velocities. The solid thick line *A* shows the atom at rest. The solid thin line *B* has the atom leaving at 185 m/s. The dashed line *C* has the atom exiting the cavity at 590 m/s. Note the difference of scales for *A* on the right, and for *B* and *C* on the left.

tons [9]. For every photon that exits the cavity through the mode there are $1+2C$ spontaneously emitted photons. This background leads to a modification of the spectrum of squeezing shown in the bottom of Fig. 3. Comparing the spectra in Fig. 2 to that of Fig. 3 a positive peak centered at the LO frequency ($\Omega=0$) has appeared, corresponding to the higher spontaneous emission.

3. Spatial distribution of atoms in the mode of the cavity

The atoms from the atomic beam are not all maximally coupled to the cavity mode. The model takes into account two effects: The spatial distribution of the atoms in the mode of the cavity, and the transit time of the atoms through the cavity. Both reduce the size of the nonclassical effects, but still permit their manifestation in the experiment. Carmichael and Sanders [31] showed that for a standing wave, Gaussian cavity mode, the distribution of atom-cavity coupling constants g is

$$P(g/g_0)=\frac{A\cos^{-1}(g/g_0)}{g/g_0}, \tag{22}$$

where A is a normalization constant that depends on the total mode volume considered. Equation (22) shows that for an atomic beam there will be many atoms weakly coupled to the cavity.

We consider the effect that this spatial distribution alone has on the size of the quantum fluctuation. We perform a weak field, quantum trajectory simulation for an ensemble of atoms at rest by first randomly distributing N atoms according to Eq. (22). We then allow this system to evolve towards a steady state with all the atoms at rest. Then we force the cavity to emit a photon. We follow the conditioned field evolution for this distribution of atoms. Finally we average the conditioned field evolution over 1000 ensembles in order to arrive at an averaged conditioned field evolution. We find a typical decrease in the size of the quantum fluctuation by at least a factor of 2 compared to that seen with the atoms maximally coupled.

Figure 4 shows a calculation of the conditional field, $h_{0\circ}(\tau)$, averaged over 1000 ensembles, each containing 190 atoms. We use the same system parameters as those used in Fig. 2, but increase the number of atoms such that Ω_0 remains the same. Notice both the reduction in the amplitude and the increase in the decay rate of the oscillation compared to Fig. 2. Nevertheless, the nonclassical features are preserved.

4. Transit time of the atoms

The atoms in the experiment are not at rest but they cross the cavity waist in typically four to five atomic lifetimes. We begin by assuming that a single atom is maximally coupled to the cavity long enough to let the system reach equilibrium. Then the atom moves out of the mode at different velocities following a cavity emission. We find two significant effects associated with this.

The first effect is to reduce the size of the normalized fluctuation. This occurs because the steady state reached by the cavity is much higher without atoms for the same input drive. This effect is enhanced in our simplified picture because, in the experiment, the total number of atoms is always nonzero. The second effect is that the decay rate of the system increases with increasing atomic velocity. This is understood in terms of a modified atomic decay rate ($\gamma_\perp$). The atom now sees a ''pulsed'' excitation that translates into an effective decay. Brecha *et al.* [23] studied the effects of this dephasing in the intensity-intensity correlations for cavity QED and found a rapid degradation of the nonclassicality as the ratio $\gamma_\parallel/2\gamma_\perp$ decreased.

Figure 5 demonstrates the qualitative effect of transit broadening due to the atomic beam by considering a single atom coupled to a cavity with parameters $(g_0,\kappa,\gamma_\perp)/2\pi=(35,8,3)$ MHz. Trace *A* shows $h_0(\tau)$ for an atom with no velocity. In contrast, traces *B* and *C* show the correlation for atoms leaving the cavity at 185 m/s and 590 m/s, respectively. The amplitude $h_0(\tau=0)$ is dramatically reduced by nearly two orders of magnitude. The change of the decay constant is also remarkable as the oscillations damp out with increasing velocity, completely disappearing at 590 m/s, a typical thermal beam velocity. This simulation gives us a

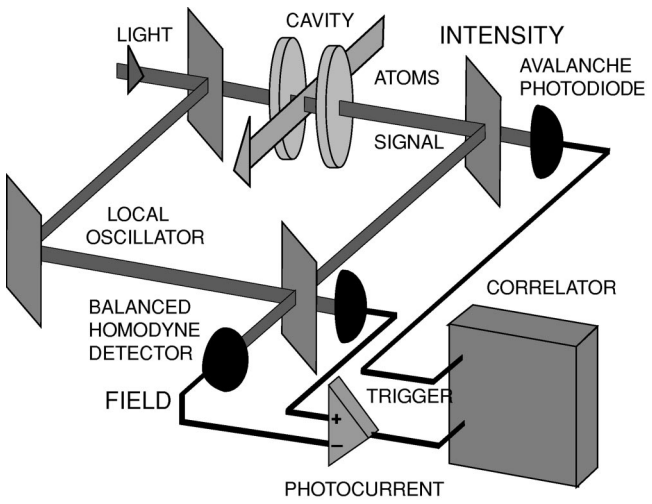

FIG. 6. Simplified diagram of the experimental setup.

qualitative understanding of effects due to atomic transit across the cavity mode, but a full quantum Monte Carlo simulation would be necessary to obtain quantitative results.

III. APPARATUS

A. Correlator

The measurement requires a homodyne measurement of the transmitted cavity signal correlated with photon detections. We implemented a modified Mach-Zehnder interferometer to perform the measurement. Figure 6 is a schematic of the experiment. Light enters the Mach-Zehnder interferometer, driving the cavity QED system on one arm and providing an LO for the balanced homodyne detector (BHD) on the other [27]. A fraction of the signal is directed to the intensity detector [avalanche photodiode (APD)]. The remaining signal is sent to the BHD. The photocurrent from the BHD is proportional to the signal field amplitude. We correlate photon detections with the BHD photocurrent to measure the field-intensity correlation. We will discuss each component of the measurement in detail below.

B. Cavity QED system

The cavity QED system consists of a beam of optically pumped Rb atoms traversing a driven high finesse Fabry-Perot cavity. This serves as the source in the field-intensity correlator. The heart of the experiment is the optical cavity. This is formed by two high reflectivity curved mirrors coated by Research Electro-Optics. Each mirror is mounted to a stainless steel holder that is inserted into a stainless steel tube with a collimating slit. Piezoelectric transducers attached to the mirror holders allow us to control the mirror spacing. During measurements, a feedback loop holds the cavity on the resonance. The cavity tube rests on a stack of sorbothane and lead which provides isolation from mechanical vibrations. The cavity defines a transverse electromagnetic Gaussian standing-wave mode (TEM_{00}) with waist $w_0=21\ \mu$m, and length $l=410\ \mu$m. We use a one-sided configuration with a 300 ppm transmission output mirror and 10 ppm transmission input mirror. The fractional solid angle subtended by the cavity mode is small enough ($\sim 10^{-3}$) that we do not have to make corrections to the atomic decay rates.

An effusive oven 35 cm from the cavity produces a thermal beam of Rb atoms in a chamber pumped by a large diffusion pump with typical operating pressures of (1×10^{-6} Torr). Collimation comes from a water cooled copper plate 5 cm from the oven opening, and a 3 mm slit 5 cm further downstream. Final collimation is provided by a 70 μm slit on the front of the cavity holder. The oven is heated to $\approx$430 K. A computer controlled feedback system maintains the temperature of the oven within ± 0.1 K. The 1-mm-wide oven opening and the slit before the cavity form a beam with an angular spread of 3.4 mrads. A welded bellows provides vibration isolation between the diffusion pump and the six-way cross containing the cavity. A liquid nitrogen cooled Cu sleeve surrounds the cavity to reduce background atomic vapor. The presence of a background atomic vapor destroys the observed correlations.

The excitation source for the experiment is a Verdi 5 pumped titanium sapphire (Ti:sapphire) laser, a modified Coherent 899-01. The laser beam is split into a signal beam and auxiliary beams for laser frequency locking, cavity locking, and optical pumping. The linewidth of the laser is less than 200 kHz over 1 sec as measured independently on a Fabry-Perot fringe with detection bandwidth of $\approx$400 kHz. The signal and lock beams are on resonance with the $5S_{1/2}$, $F=3\rightarrow 5P_{3/2}$, $F=4$ transition of ^{85}Rb at 780 nm. A double passed acousto-optic modulator in the laser lock allows us to adjust its frequency around the Rb resonance.

An optical pumping beam of diameter 2 mm, parallel to the cavity mode, intersects the atomic beam 1 cm before the atoms enter the cavity. The atoms are excited into the strong cycling transition $5S_{1/2}$, $F=3$, $m_F=3\rightarrow 5P_{3/2}$, $F=4$, $m_F=4$. A 2.5 G uniform magnetic field applied along the axis of the cavity provides a quantization axis such that the circular polarization of the optical pumping beam takes all the atoms into the ground-state magnetic sublevel $F=3$, $m_F=3$.

An electro-optic modulator generates frequency sidebands on the lock beam. The reflected lock beam is used to hold the cavity on resonance. During data collection, we send the beam through a chopper wheel that alternately passes the lock beam and opens the path from the cavity to the photon counting detectors at $\approx$1.1 kHz. The lock beam is blocked for a longer time than the signal path is open, ensuring that no lock beam light enters the cavity while we collect data. The duty cycle of signal open/closed is typically 1/3.

The lock and signal beams have orthogonal linear polarizations when they are combined at a nonpolarizing beam splitter before the cavity. The resulting beam is sent through a $\lambda/4$ plate and mode matched into the cavity with more than 90% of the signal beam intensity into the TEM_{00} mode. The polarization of the signal is in the same sense as that of the optical pumping beam. On the output side of the cavity, the beam passes through another $\lambda/4$ plate to convert back the lock and signal beams into orthogonal linear polarization. A polarizing beam splitter sends the lock beam to a photomultiplier, for monitoring purposes. The signal beam is directed

to the correlator, passing through the chopper wheel on the way towards the avalanche photodiodes. We typically send between 50% and 85% of the signal emitted from the cavity to the homodyne detectors. The remaining 50%–15% of the signal is directed to the avalanche photodiodes.

The three rates for the atom-cavity coupling, cavity decay, and atomic decay of our apparatus are $(g_0,\kappa,\gamma_\perp)/2\pi = (12,8,3)$ MHz, with $C_1=3$ and $n_0=0.08$ placing it in the strong-coupling regime of cavity QED. We operate with an average intracavity field less than that of one photon.

C. Balanced homodyne detection

Homodyne detection permits the detection of a signal field by interfering it with the LO, a strong field at the same frequency as the signal, of known intensity and fixed phase. This allows a phase-sensitive measurement of the signal field quadratures and also amplifies weak signals by the local oscillator field amplitude. The local oscillator and the signal are derived from the same laser beam, which ensures they have the same initial phase.

1. Mach-Zehnder interferometer

A Mach-Zehnder interferometer is used to separate the laser into the local oscillator and a signal beam which follow separate paths but maintain a constant relative phase. A balanced Mach-Zehnder consists of an input 50/50 beam splitter that splits an incoming beam into two paths, which are recombined at the output 50/50 beam splitter. To ensure maximum interference, the two beams must have the same size and wave-front curvature. We can quantify the spatial overlap by the fringe visibility as the relative phase between the two arms varies. Only the fraction of the signal given by the visibility is detected in the mode defined by the local oscillator. We mode match the local oscillator to the signal and typically achieve a visibility of 0.80 or better.

2. Phase control

We control the relative phase of the LO and signal by adjusting the path difference of the two arms with a piezo-actuated mirror (PZT). Control of the phase between the LO and the signal is critical in the homodyne technique we employ. Since we have to perform repeated averages to reduce the intrinsic shot noise, a drifting phase will average out the signal. We actively stabilize the interferometer length with a feedback system.

We use a thermally stabilized He-Ne laser ($\lambda=633$ nm) or a diode laser ($\lambda=640$ nm) locked using FM sidebands to an iodine cell. The cavity QED system is transparent to these red wavelengths, but they form fringes at the Mach-Zehnder (MZ) output. An edge filter separates the 780 nm and red wavelengths after the MZ output beam splitter. We apply a small dither at 5 kHz to the mirror. We send the amplified output of a (red) photodiode to a lock-in amplifier (Stanford Research SR510) to obtain an error signal. This allows us to maintain the MZ length such that it sits at a red fringe maximum or minimum. We can adjust the phase by locking the length to different red fringes, at either a maximum or minimum. The IR phase can be adjusted in steps of $\delta\theta_{IR}=146°=(180°\times 633/780)$. There is also an optical path delay that can be mechanically adjusted to bring the IR and red in phase at a particular fringe. The path lengths of the two arms are nearly equal to minimize the effect of frequency drift of the red laser.

3. Amplitude detectors

The combined signal and LO field is directed to a pair of biased silicon photodiodes (Electro-Optics Technology EOT 2030) configured as a BHD [27]. These are characterized by low noise, fast response time (<300 ps), and quantum efficiency of $\eta\approx 85\%$ at 780 nm.

The ac coupled current from the photodiodes is amplified and subtracted. The current from a detector first passes through a bias T that filters dc components less than 100 kHz. The dc component gives a direct measure of the local oscillator current. The filtered current is then sent to a low-noise amplifier (Minicircuits ZFL-500LN) that amplifies the power by ≈ 20 dB over a frequency range from 100 kHz to 500 MHz. The currents from the two photodiodes are then subtracted in a splitter/combiner (Minicircuits ZFSCJ-2-1). Subtracting the two currents from the photodiodes allows common mode rejection of local oscillator intensity noise (technical noise) [27]. The signal in one output port of the MZ beam splitter acquires a π phase shift after reflection from the coated beam splitter surface, so the signals add in the combiner. The combined signal is then amplified 40 dB and low-pass filtered with 70 MHz. The output is then sent to the digital oscilloscope (Lecroy 9354A) for data collection.

We characterize the detector response by looking at the output in a spectrum analyzer. A typical local oscillator power of 15 mW per detector produces 10 dB of shot noise above the electronic noise floor with a 300 kHz bandwidth. Blocking one detector or the other results in a factor of 2 reduction (3 dB). No bright lines are evident over the detection window of 10–70 MHz.

We optimize the common mode rejection by balancing the photocurrents. The detectors are aligned to couple as much as possible and to reduce backscatter light. Additional balancing of the detector current is accomplished by placing a small attenuator (1 dB) in the electronic path of one of the signals before the current subtraction.

4. Intensity Detectors

The intensity detectors are arranged as a photon correlator that consists of two APDs EG&G SPCM-AQ-151 behind an unpolarized 50/50 beam splitter. These detectors have a quantum efficiency of 50%, less than 50 Hz dark count rate, and a dead time of 30 ns. The detector electronics produce a transistor-transistor logic (TTL) pulse for each photon detection. An unfortunate property of APDs is the light emitted from the APD during the avalanche process [28]. Since the detectors are mode matched to the cavity output, light emitted from the one APD can reflect from the cavity and enter the other APD, causing false counts. The emission is broadband and unpolarized, so a combination of spectral filters and polarizers in front of the APDs alleviates the problem. The spectral filters are an Andover 10-nm-wide interference

filter with 88% peak transmission, and a piece of antireflection coated Schott RG-9 glass, which significantly attenuates wavelengths greater than 1 μm. The total transmission at 780 nm is 84%.

When we measure the intensity correlation function of the system, we let pulses from the start APD serve as the triggers for a Lecroy 3377 time to digital converter (TDC) that registers the arrival time of up to 16 pulses from the stop APD with 0.5 ns resolution. The TDC registers photodetections for a 1 μsec window per start. The timing data is transferred across a CAMAC crate to a Lecroy 4302 memory module that stores up to 16 000 hits. When the memory is full, the data is transferred over a GPIB bus to a computer. A program controls the data collection by creating both a histogram of the data and corresponding plot.

The pulses from the APDs pass through a series of gates, logic boxes, and delays before arriving at the TDC. The pulses from the start detector are gated so that additional pulses from the start detector are blocked from retriggering the TDC. Both the start and stop pulses are then gated with a signal derived from the optical chopper wheel so that pulses get to the TDC only when the signal is open and the lock beam blocked. The stop pulses are delayed by $\approx$400 ns to allow us to see zero delay coincidences. A copy of the pulses from each detector goes to a Stanford Research Systems SR400 photon counter to measure the count rates from each APD. These rates yield the mean intensity of the light emitted from the cavity after correcting for efficiencies and linear losses.

A small fraction of the LO reflects off the BHD photodiodes and can bounce off the cavity into the APDs, causing false starts. A Faraday rotator inserted before the output beam splitter of the Mach-Zehnder interferometer reduces this to a negligible level.

D. Correlator data acquisition

We sample the homodyne current with a digital oscilloscope triggered by photon detections registered at the APDs. The photon counting apparatus used for correlation measurement produces the trigger. Instead of doing time correlations, we take the nuclear inline module (NIM) signals from the two APDs and logically OR them. The combined trigger is gated by the lock/signal chopper gate and is delayed by $\approx$50 ns. The total delay between the homodyne input and the APD trigger arriving at the oscilloscope including optical path differences is $\approx$150 ns.

The digital oscilloscope samples the BHD photocurrent over a 500 ns window at 2 G/s with an 8 bit analog to digital (AD) converter. The oscilloscope performs a summed average of the triggered samples. Typically we average for up to 5×10^4 samples.

The square root of the number of samples N_s sets a limit to the signal to noise ratio achievable. The AD converter has 8 bit resolution, so the minimum standard deviation is 1 bit. Assuming that originally the noise is as large as the digitizer allows, then the number of averages will reduce the size of the noise by the number of samples N_s, until the noise reaches a limit at $N_s=256^2$.

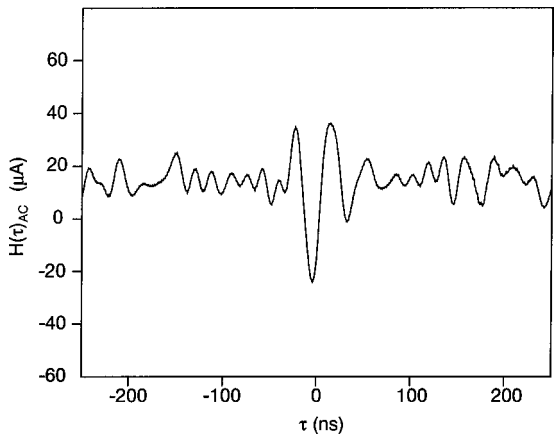

FIG. 7. Averaged conditioned photocurrent.

We need to have as much sampling resolution as possible, but we can only average for 256^2, which creates a sample of finite length that is too short to average the low-frequency oscillations present in the shot noise. A filter limiting the detection bandwidth to frequencies above 100 kHz can cause the average ac photocurrent to show an offset, this is artificial and can be further aggravated by problems of imperfect cancellation at low frequency of common mode intensity fluctuations of the local oscillator. The addition of a 6 MHz high pass filter significantly reduces this problem.

IV. RESULTS

We initially characterize the system with intensity correlation measurements. With this system, we can observe sub-Poissonian antibunching at a low intracavity field. If the beam is not perpendicular to the cavity mode, we compensate for the resulting Doppler shift by adjusting the laser frequency to minimize the transmitted intensity and to maximize the size of the nonclassical effect seen in the photon correlations [15]. When we have obtained a nonclassical $g^{(2)}(\tau)$, we switch to the field measurement. We send a fraction of the signal to the BHD and then lock the Mach-Zehnder output. We then begin sampling the homodyne photocurrent.

To characterize the intracavity intensity, we use the count rates measured by the APDs. To calculate the intracavity intensity, we first determine the flux at the cavity output, by taking into account the 50/50 beam splitter in front of the APDs, the quantum efficiency (0.5), the filter transmission (0.85), the signal/lock duty cycle (0.35), and the splitting fraction η of the beam splitter directing the signal to the BHD and APD's. We make use of the following relation from OB to determine the intracavity intensity normalized by the saturation photon number from the power P determined at the cavity output: $X=n/n_0=3P/\pi w_0^2 I_{sat} T$. $I_{sat}=\pi\hbar\omega/(3\tau\lambda^2)$ (1.7 mW/cm^2 in Rb) is the saturation intensity of the atom with transition frequency ω and lifetime τ. T is the output mirror transmission, and the output flux F relates to the intracavity photon number through $F=2\kappa\langle\hat{a}^\dagger\hat{a}\rangle$.

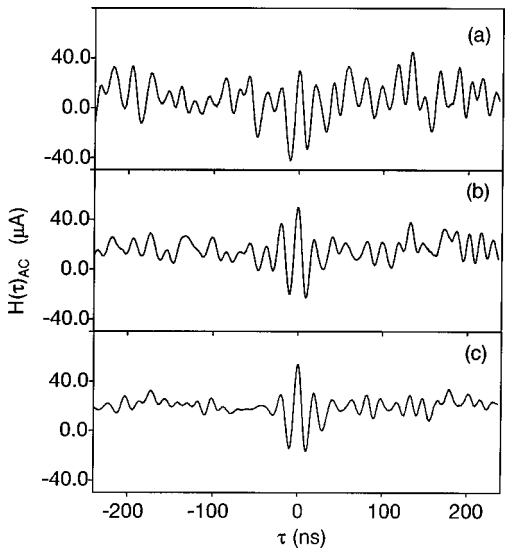

FIG. 8. Average conditional photocurrent for (a) 6000, (b) 18 000, and (c) 59 000 samples.

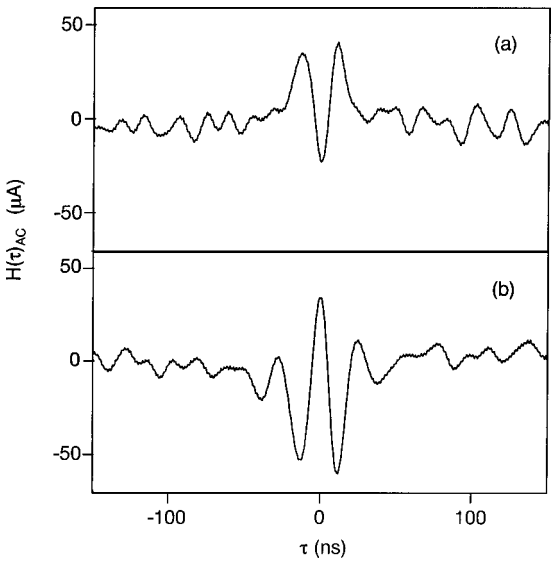

FIG. 9. Plots (a) and (b) are un-normalized homodyne averages with a phase difference of 146°.

A. Signals

Figure 7 depicts a typical averaged conditioned photocurrent from the BHD detector. $\tau=0$ is defined by APD photodetection, which triggers the scope to average the BHD photocurrent. The measured BHD photocurrent is a combination of events with and without a cavity signal. If, after the initial photodetection there are no remaining excitations in the cavity, the BHD signal will contain only shot noise from the local oscillator. If, however, there is energy in the system, as given by the different coefficients of the conditional state in Eq. (17), the evolution of the field will be recorded in the photocurrent of the BHD. We optimize the BHD by an appropriate choice of η (fraction sent to BHD) and operation point of the system. This is necessary, given the finite number of averages that we can get.

The decaying oscillation is the evolution of the cavity field back to steady state. With the system initially in its steady state, Eq. (14), a photodetection at the APD reduces the cavity state, Eq. (17). Physically, this photodetection tells us that an excitation has escaped through the cavity mirror and was detected in the APD. Then the system has to evolve back to steady state by exchanging the remaining excitation between the atoms and the cavity at the vacuum Rabi frequency Ω_0. This exchange of excitation is described by the time-dependent amplitude, $\mathcal{A}F(\tau)$ in Eq. (19). This is the evolution recorded in the BHD photocurrent.

Figure 8 depicts the reduction of the shot noise as the signal is averaged. Since the cavity output is mixed with a local oscillator that is at least eight orders of magnitude more intense, the shot noise fluctuations in the local oscillator dominate over the signal. This requires averaging. Figure 8(a) shows the result after 6000 averages with the random shot-noise fluctuations averaged to a level where they are approximately equal to the cavity signal. In Fig. 8(b), the signal is more evident after 18 000 averages, and finally Fig. 8(c) shows the random fluctuations averaged to a level where the cavity signal is clearly distinguishable after 59 000 samples. The survival of the signal after many averages is due to the fact that every APD photodetection prepares the cavity QED system in the same state described by Eq. (17), which then evolves back to equilibrium in a time set by the decay parameters of the system.

The BHD measures the interference between the local oscillator and the emitted cavity field, which depends on the relative phase between them [Eq. (3)]. Figure 9 shows the change in the average ac photocurrent (voltage across 50 Ω) for two different local oscillator phases with the system operates at low intensity. When the relative phase is changed by $146° \approx 180°$ (see Sec. III B 2 on phase control) the sign of the interference changes. The apparent change in the dc is due to the mechanisms discussed previously. Normalization is discussed in detail in the following section. Notice that the value of the measured field at $\tau=0$ in Fig. 9(a) is less than the steady-state value. This is evidence of a nonclassical field, since it violates the lower bound of the Eq. (9) inequality. This nonclassical feature demonstrates that the field fluctuations are anticorrelated with the conditioning photon that allows for the dynamics to show explicitly in this measurement. Rather than showing random field fluctuations, we see explicit evidence of the projection of the polarization field out of phase with the intracavity field.

We have performed a series of checks on our measurement. These included blocking the atomic beam and triggering the digital storage oscilloscope from a thermal source instead of from photodetections from the output of the cavity QED system. The field correlation disappeared in both cases. We also have directed varying fractions of the signal to the BHD and observed the expected scaling in the size of the signal.

The fluctuations are always due to the emission of a single photon. The size of the saturation photon number n_0 in our experiment is less than 1. Figure 10 shows data taken at an intracavity intensity $n/n_0=0.30$. This corresponds to a mean intracavity photon numbers of 0.027, in the low-intensity

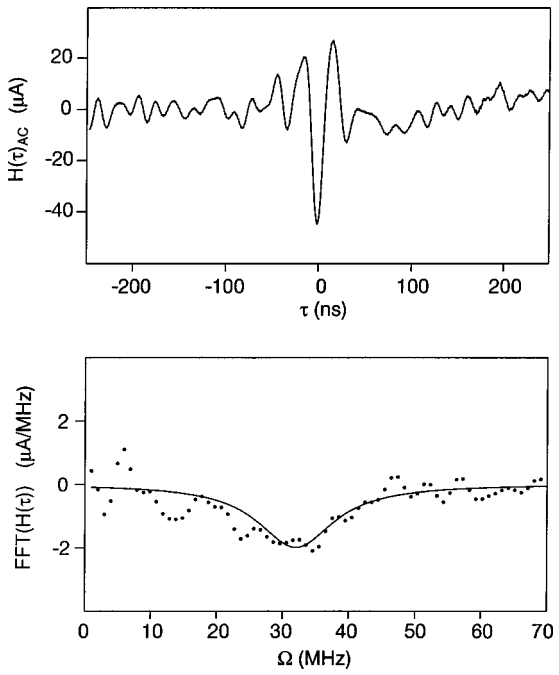

FIG. 10. Low-intensity ($n/n_0=0.3$) field correlation and FFT.

regime. The top trace is the unnormalized correlation function $H(\tau)$, it shows nonclassical behavior, as the correlation is minimal at $\tau=0$, the bottom trace shows the FFT of the top trace. Equation (6) establishes the relationship between the correlation function and the spectrum of squeezing, so the bottom trace is proportional to the spectrum of squeezing and shows a dip at the vacuum Rabi Splitting Ω_0 of the system. There is qualitative agreement between these traces and those in Fig. 2. The amplitude of the field should be the greatest at $\tau=0$ as given by the initial jump Eq. (21) in the field caused by the escape of a photon from the system. The continuous line in the FFT has the functional form predicted by the low-intensity theory (see Ref. [9]).

B. Normalization

The field correlation defined by Eq. (5) is normalized to the mean field. Obtaining a proper normalization requires precise knowledge of the average mean field. Our detection system is ac coupled, so we have to determine the mean steady-state field in some other manner.

We determine the proper dc level and normalization by comparing the expected shot noise after averaging with the measured noise in our data. The knowledge of the averaging procedure allows us to extract the normalized correlation. The noise amplitude for the normalized correlation is

$$\delta h=\frac{1}{2\langle\hat{a}\rangle\sqrt{2\kappa\eta}}\sqrt{\frac{B\kappa}{2N_s}}, \tag{23}$$

where N_s is the number of starts, κ is the cavity bandwidth, B is the detector bandwidth in units of the cavity bandwidth κ, η is the fraction of the output power sent to BHD, and $\langle a\rangle$ is the mean intracavity field.

We assume the data can be scaled with two constants Ξ and Υ, such that

$$h(\tau)=\Xi h_{\text{expt}}(\tau)+\Upsilon. \tag{24}$$

For $\tau\rightarrow\infty$, Eq. (24) is equal to 1,

$$\Xi h_{\text{expt}}(\infty)+\Upsilon=1. \tag{25}$$

We can determine Ξ by noting that $\Xi\,\delta h_{expt}=\delta h$ and assuming that the coherent transmission dominates the incoherent transmission ($\langle a\rangle\approx\sqrt{\langle\hat{a}^\dagger a\rangle}$),

$$\Xi\approx\frac{1}{4\,\delta h_{\text{expt}}}\sqrt{\frac{B}{\langle\hat{a}^\dagger\hat{a}\rangle\,\eta N_s}}. \tag{26}$$

Υ can then be recovered from Eq. (25). This method is based on measured quantities from the experiment. We record the number of starts on the scope. The intracavity intensity and η are obtained from the measured flux at the APDs, and the detection bandwidth is determined by the 70-MHz low-pass filter. The noise amplitude δh_{expt} is determined by taking the standard deviation of the un-normalized data.

A second approach to the normalization of $h(\tau)$ uses our knowledge that the normalized field correlation is the square root of the intensity correlation $g^{(2)}(\tau)$ in the weak-field limit. This allows us to determine a dc level for the raw field measurement that properly scales the normalized field correlation. The comparison to the square root of $g^{(2)}(\tau)$ is not completely valid because this data is not taken in a weak-field regime.

Finally, we can normalize by calculating the dc field expected from the measured photon flux from the cavity. From the measured flux, the expected dc voltage level can be calculated. Adding this level, then dividing by the mean level normalizes the correlation data to a long time mean of unity.

The difference between the first method or normalizing by the expected noise and the other two is that we have only included the fraction of the light directed to the BHD without including the signal LO overlap, quantum efficiency, and additional losses (mainly from the Faraday isolator transmission). We employ the first method for our normalized results presented here.

Figure 11 shows $h(\tau)$ for a large intracavity intensity ($n/n_0=1.2$). The size of the field amplitude is nearly unchanged, but the background has appeared. The intensity correlation for an input intensity within 10% of that for the field measurement shows only classical fluctuations. Qualitatively this conditional field agrees with that in Fig. 3 where the increased drive causes many more spontaneous emissions, which can interrupt the evolution of the system back to steady state following the escape of a photon as set by Eq. (21). Reiner *et al.* in Ref. [9] study the effects of spontaneous emission in greater detail. The dashed area in Fig. 11 marks the limits from the Schwartz inequalities in Eqs. (9) and (12). The field is clearly nonclassical.

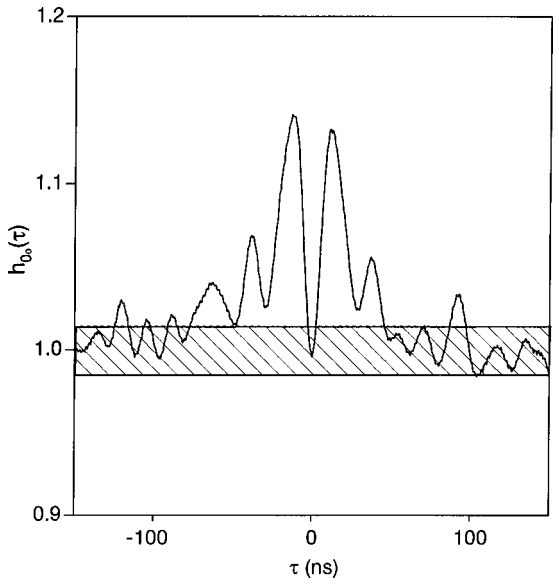

FIG. 11. Normalized field correlation for an in-phase field. $N=13$ and $n/n_0=1.2$. The dashed region is classically allowed.

C. Spectrum of squeezing

The Fourier transform of the normalized field correlation times the source flux F yields the spectrum of squeezing [Eq. (6)]. A single time domain measurement of the field fluctuations yields the entire frequency domain spectrum of squeezing. To compute the spectrum in Fig. 12 we use the normalized data of Fig. 11. First, we symmetrize the time series of the data so that the data is ordered in an array with positive times with the negative times following. We take the real part of the fast Fourier transform and multiply the result by the time resolution of the data and by twice the flux F determined from the measured rates at the APDs and the measured efficiencies. This cancels the time unit introduced by the FFT and ensures that the spectrum is dimensionless. We multiply by a factor of 2 instead of 4 because our Fourier transform is performed for both positive and negative times, while the squeezing spectrum is defined for positive times. The solid line is the squeezing spectrum with the noise filtered out.

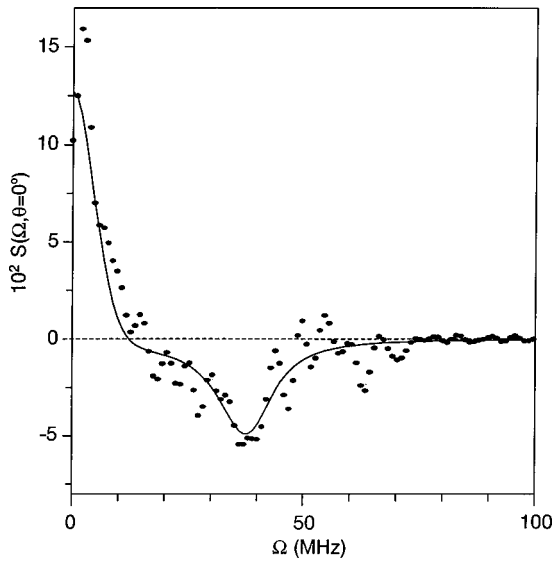

FIG. 12. Squeezing spectra for cavity system with $n/n_0=1.2$, and source flux $F=10.9\times10^6$ photons/sec.

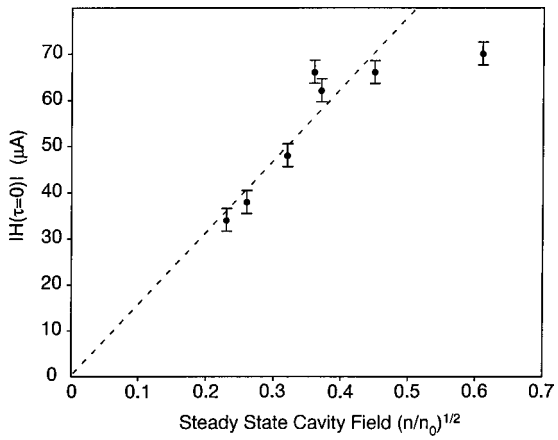

FIG. 13. Amplitude of the oscillating conditional photocurrent $H(0)$ as a function of the square root of the normalized field.

We observe squeezing below the standard quantum limit (or the shot-noise level) at Ω_0 the coupling frequency of the system. At this frequency, the field exhibits squeezing of $\approx 5\%$. The positive component centered at zero is a result of spontaneous emission noise [9] and is in qualitative agreement with that obtained in Fig. 3.

D. Amplitude of signal

We have measured the conditional field evolution for several different values of the cavity input intensity. Figure 13 shows the amplitude of the measured oscillation $H(0)$ as a function of this driving intensity. The response is approximately linear for low driving intensities, a relationship that is lost for stronger drives. From OB studies we know that the driving field and the transmitted field are linearly related by $1+2C$. We infer the driving field from the measured photon count rates. Quantum trajectory simulations [9] indicate that the deviation from linearity of the relationship is due in part to spontaneous emission. There is also an increased probability for the system to have more than two excitations. The spontaneous emission events, $1+2C$ times more common than the escape out of the cavity only show their presence indirectly in the correlation function as they escape through other modes outside the preferred one.

For low enough drives, the amplitude of the conditional field is given by Eq. (21). Note that this is λ the coefficient of $|1\rangle$ in Eq. (17). This term describes the probability for occupation of the cavity mode by a single photon. Our measurements record the evolution of this coefficient.

V. CONCLUSION

The strong coupling between the cavity and the atom in cavity QED permits us to follow the dynamics of the field on a time scale many orders of magnitude slower than the optical frequencies using the field-intensity correlation. The strong coupling creates a regime in which a single photon

fluctuation is an order of magnitude larger than the mean intracavity photon number. In this sense cavity QED is ideal for the study of the time evolution of the field at the subphoton level.

The remarkable feature of the cavity QED system is that the detection of a photon projects the system into a well-defined quantum-mechanical state that evolves in time in a phased way. The field-intensity correlation measurement uses this feature to observe this evolution in the emitted field. By triggering the homodyne field detector on the photon detection, we can recover this subphoton field fluctuation from the large shot-noise background. The time domain field correlation provides us with the information to construct the squeezing spectrum for the source in an efficiency-independent manner.

Future studies may try to map out a full phase-space picture of the field as it evolves in time. This would involve sampling the field at various phases and performing some type of tomographic reconstruction to arrive at a quasiprobability distribution, such as the Wigner distribution [29].

The conditional homodyne technique may have more general application to study other sources, both classical and nonclassical, since the information obtained through this field-intensity correlation approach complements and synthesizes the one coming from intensity-intensity correlations (particle aspect) or squeezing (wave aspect).

ACKNOWLEDGMENTS

We would like to acknowledge the interest and help in this work of H. J. Carmichael and P. Rice. This work was supported by NSF and NIST.

[1] R. Hanbury-Brown and R.Q. Twiss, Nature (London) **177**, 27 (1956).
[2] H.J. Kimble, M. Dagenais, and L. Mandel, Phys. Rev. Lett. **39**, 691 (1977).
[3] L. Mandel and E. Wolf, *Optical Coherence and Quantum Optics* (Cambridge University Press, New York, 1995).
[4] R.E. Slusher, L.W. Hollberg, B. Yurke, J.C. Mertz, and J.F. Valley, Phys. Rev. Lett. **55**, 2409 (1985).
[5] Squeezed Light, J. Mod. Opt. **34**, 709 (1987) (special issue, edited by R. Loudon and P.L Knight).
[6] Squeezed States of the Electromagnetic Field, J. Opt. Soc. Am. B **4**, 1450 (1987) (special issue, edited by H.J. Kimble and D.F. Walls).
[7] H.J. Carmichael, H.M. Castro-Beltran, G.T. Foster, and L.A. Orozco, Phys. Rev. Lett. **85**, 1855 (2000).
[8] G.T. Foster, L.A. Orozco, H.M. Castro-Beltran, and H.J. Carmichael, Phys. Rev. Lett. **85**, 3149 (2000).
[9] J.E. Reiner, W.P. Smith, L.A. Orozco, H.J. Carmichael, and P.R. Rice, J. Opt. Soc. Am. B **18**, 1911 (2001).
[10] H.M. Wiseman, Phys. Rev. A **65**, 032111 (2002).
[11] A. Denisov, H. M. Castro-Beltran, and H. J. Carmichael Phys. Rev. Lett. **88**, 243601 (2002).
[12] *Cavity Quantum Electrodynamics*, edited by P. Berman (Academic Press, Boston, 1994).
[13] G. Rempe, R.J. Thompson, R.J. Brecha, W.D. Lee, and H.J. Kimble, Phys. Rev. Lett. **67**, 1727 (1991).
[14] S.L. Mielke, G.T. Foster, and L.A. Orozco, Phys. Rev. Lett. **80**, 3948 (1998).
[15] G.T. Foster, S.L. Mielke, and L.A. Orozco, Phys. Rev. A **61**, 053821 (2000).
[16] M.G. Raizen, L.A. Orozco, M. Xiao, T.L. Boyd, and H.J. Kimble, Phys. Rev. Lett. **59**, 198 (1987).
[17] L.A. Orozco, M.G. Raizen, Min Xiao, R.J. Brecha, and H.J. Kimble, J. Opt. Soc. Am. B **4**, 1490 (1987).
[18] D.M. Hope, H.A. Bachor, D.E. McClelland, and A. Stevenson, Appl. Phys. B: Photophys. Laser Chem. **55**, 210 (1992).
[19] B. Yurke and D. Stoler, Phys. Rev. A **36**, 1955 (1987).
[20] A.I. Lvovsky, H. Hansen, T. Aichele, O. Benson, J. Mlynek, and S. Schiller, Phys. Rev. Lett. **87**, 050402 (2001).
[21] Hua Deng, Daniel Erenso, Reeta Vyas, and Surendra Singh, Phys. Rev. Lett. **86**, 2770 (2001).
[22] H.J. Carmichael, R.J. Brecha, and P.R. Rice, Opt. Commun. **82**, 73 (1991).
[23] R.J. Brecha, P.R. Rice, and M. Xiao, Phys. Rev. A **59**, 2392 (1999).
[24] H.J. Carmichael, J. Opt. Soc. Am. B **4**, 1588 (1987).
[25] L. A. Lugiato, in *Progress in Optics*, edited by E. Wolf (North-Holland, Amsterdam, 1984), Vol. XXI, pp. 69–216.
[26] H. A. Bachor, *A Guide to Experiments in Quantum Optics* (Wiley-VCH, New York, 1998).
[27] H.P. Yuen and V.W.S. Chan, Opt. Lett. **8**, 177 (1983); **8**, 345(E) (1983).
[28] A.L. Lacaita, F. Zappa, S. Bigliardi, and M. Manfredi, IEEE Trans. Electron Devices **ED40**, 577 (1993).
[29] U. Leonhardt, *Measuring the Quantum State of Light* (Cambridge University Press, New York, 1997).
[30] J.P. Clemens and P.R. Rice, Phys. Rev. A **61**, 063810 (2000).
[31] H.J. Carmichael and B.C. Sanders, Phys. Rev. A **60**, 2497 (1999).